J. Am. Chem. Soc. **1990**, *112*, 7498-7502

Layer-by-Layer Nanometer Scale Etching of Two-Dimensional Substrates Using the Scanning Tunneling Microscope

Bruce Parkinson

Contribution No. 5399 from the Central Research and Development Department, E. I. DuPont de Nemours & Co., E328/216, Wilmington, Delaware 19898.
Received March 9, 1990

Abstract: The scanning tunneling microscope can be used to sequentially etch single molecular layers from the surface of two-dimensional materials (i.e., $SnSe_2$, $TiSe_2$, and $NbSe_2$). Etching occurs by the nucleation and growth of holes in the region of the sample rastered by the tip under normal conditions of tunneling bias and current. In the case of etching $NbSe_2$, triangular etch pits are formed in the initial etching stages. The mechanism for the etching process is unknown at this point although four reasonable mechanisms are proposed. Several submicron complex structures have been prepared as well as a structure as small as 25 × 25 × 1.2 nm.

The scanning tunneling microscope (STM) has become a useful tool for studying atomic resolution topography and electronic structure of conducting and semiconducting substrates. The manipulation of matter on nearly atomic scales was also discussed as a potential application early in the development of the STM, however much of this promise remains unfulfilled. There have been some reports of deliberate creation of small structures by using the STM. Single atom and single molecule manipulation has been shown in several instances.[1,2] At very high tip biases an electron beam resist can be exposed via field emission from the tip.[3,4] Metal deposition from an organometallic gas is another approach.[5-7] Protrusions have been formed on metallic glasses by local heating.[8,9] Applying voltage pulses over gold substrates can result in 2-nm features,[10-12] while larger marks can be made with mechanical indentation.[13] Due to the high surface mobility of gold, small marks such as those described are filled in within minutes after creation. Recently a technique for writing permanent features on graphite or MoS_2 has been described which uses large voltage pulses of 3-8 V to make holes 2-6 nm in diameter.[14] A similar technique was also applied to a high T_c superconductor.[15] Recently, nanometer-sized structures on the conducting oxide $Rb_{0.3}MoO_3$ were created by using small tip to sample separations.[16] We report the use of the STM to etch two-dimensional metal chalcogenide substrates in a very controlled layer-by-layer fashion by simply rastering the tip with normal tunneling biases (±0.05 - 1.5 V) and currents (0.1-5 nA). We and others[17-24] have previously shown that these 2D materials are nearly ideal substrates for STM studies in air due to their easily renewable (via simple cleavage) and inert (to O_2 and H_2O) van der Waals surfaces. The atomic flatness over large areas and the variety of electronic properties available within the structural motive (metals to large band gap semiconductors) are advantagenous for both fundamental and applied STM studies.

Figure 1 shows the time evolution of hole nucleation and growth on the surface of an n-$SnSe_2$ crystal during rastering of the STM tip in air at 0.66 nA and 480 mV. The growth of the holes continues until an entire layer is removed whereupon the next layer begins hole nucleation and the process repeats. In many cases the image of the substrate remains clear during the etching process, but it can become "fuzzy" during periods of rapid etching. It is clear from observing the process that sharp features and islands are etched more rapidly than smooth edges. Analysis of the depth information in a constant current scan of an etched area reveals that the step heights observed are, within experimental error, all multiples of the layer thickness of the 2D substrate being etched. Since the *c*-axis parameter (X-M-X sandwich thickness, the basic structure where M is a metal and X is sulfur, selenium, or tellurium) of the layered materials can be known to great accuracy (±0.001 Å) from diffraction techniques, we presume that the hole depth will also be known to similar accuracy by simply counting the number of layers which have been removed. Variation in the size and position of the square raster pattern produces rather complex features such as the inscribed squares shown in Figure 2. Continuous scanning for about 8 h over a given region has allowed us to fabricate 500-nm square holes as many as 20 molecular layers deep (12.3 nm); however, much deeper structures could have been made if we had continued scanning.

The nucleation appears to occur at defects or dopant sites but at a rate less than that for the growth of holes on high quality crystalline substrates. In some cases, perhaps due to highly doped or defective areas of the crystal, the nucleation rate exceeds the hole expansion rate, and deep irregular features are etched still clearly showing multiple layers (Figure 3). The initiation of nucleation on a small area and the growth rate of a nucleated hole appear to be the limiting factors for preparing extremely small

(1) Becker, R. S.; Golovchenko, J. A.; Swartzentruber, B. S. *Nature* **1987**, *325*, 419.
(2) Foster, J. S.; Frommer, J. E.; Arnett, P. C. *Nature* **1988**, *331*, 324.
(3) McCord, M. A.; Pease, R. F. W. *J. Vac. Sci. Technol. B* **1986**, *4*, 86.
(4) McCord, M. A.; Pease, R. F. W. *J. Vac. Sci. Technol. B* **1988**, *6*, 293.
(5) McCord, M. A.; Kern, D. P.; Chang, T. H. P. *J. Vac. Sci. Technol. B* **1988**, *6*, 1877.
(6) Ehrichs, E. E.; Yoon, S.; de Lozanne, A. L. *Appl. Phys. Lett.* **1988**, *53*, 2287.
(7) Silver, R. M.; Ehrichs, E. E.; de Lozanne, A. L. *Appl. Phys. Lett.* **1987**, *51*, 247.
(8) Staufer, U. et al. *J. Vac. Sci. Technol. A* **1988**, *6*, 537.
(9) Ringger, M.; Hidber, H. R.; Schlogl, R.; Oelhafen, P.; Guntherodt, H. J. *Appl. Phys. Lett.* **1985**, *46*, 832.
(10) Emch, R.; Nogami, J.; Dovek, M. M.; Lang, C. A.; Quate, C. F. *J. Appl. Phys.* **1989**, *65*, 79.
(11) Schneir, J.; Sonnenfeld, R.; Marti, O.; Hansma, P. K.; Demuth, J. E.; Hamers, R. J. *J. Appl. Phys.* **1988**, *63*, 717.
(12) Schneir, J.; Hansma, P. K. *Langmuir* **1987**, *3*, 1025.
(13) Jaklevic, R. C.; Elie, L. *Phys. Rev. Lett.* **1988**, *60*, 120.
(14) Albrecht, T. R.; Dovek, M. M.; Kirk, M. D.; Lang, C. A.; Quate, C. F.; Smith, D. P. E. *Appl. Phys. Lett.* **1989**, *55*, 1727.
(15) Heinzelmann, H.; Anselmetti, D.; Wiesendanger, R.; Guntherodt, H.-J.; Kaldis, E.; Wisard, A. *Appl. Phys. Lett.* **1988**, *53*, 2447.
(16) Garfunkel, E.; Rudd, G.; Novak, D.; Wang, S.; Ebert, G.; Greenblatt, M.; Gustafsson, T.; Garofalini, S. H. *Science* **1989**, *246*, 99.
(17) Tang, S. L.; Kasowski, R. V.; Parkinson, B. A. *Phys. Rev. B* **1989**, *39*, 9987.
(18) Dahn, D. C.; Watanabe, M. O.; Blackford, B. L.; Jericho, M. H. *J. Appl. Phys.* **1987**, *63*, 315.
(19) Coleman, R. V.; Drake, B.; Hansma, P. K.; Slough, G. *Phys. Rev. Lett.* **1985**, *55*, 394.
(20) Sarid, D.; Henson, T. D. *Appl. Phys. Lett.* **1988**, *52*, 2252.
(21) Weimer, M.; Kramar, J.; Bai, C.; Baldeschwieler, J. D. *Phys. Rev. B* **1988**, *37*, 4292.
(22) Wu, X.-L.; Zhou, P.; Lieber, C. M. *Nature* **1988**, *35*, 55.
(23) Tokumoto, H.; Bando, H.; Mizutani, W.; Okano, M.; Ono, M.; Murakami, H.; Okayama, S.; Ono, Y.; Watanabe, K.; Wakiyama, S.; Sakai, F.; Endo, K.; Kajimura, K. *Jpn. J. Appl. Phys.* **1986**, *25*, L621.
(24) Parkinson, B. A. *J. Am. Chem. Soc.* **1990**, *112*, 1030.

0002-7863/90/1512-7498$02.50/0

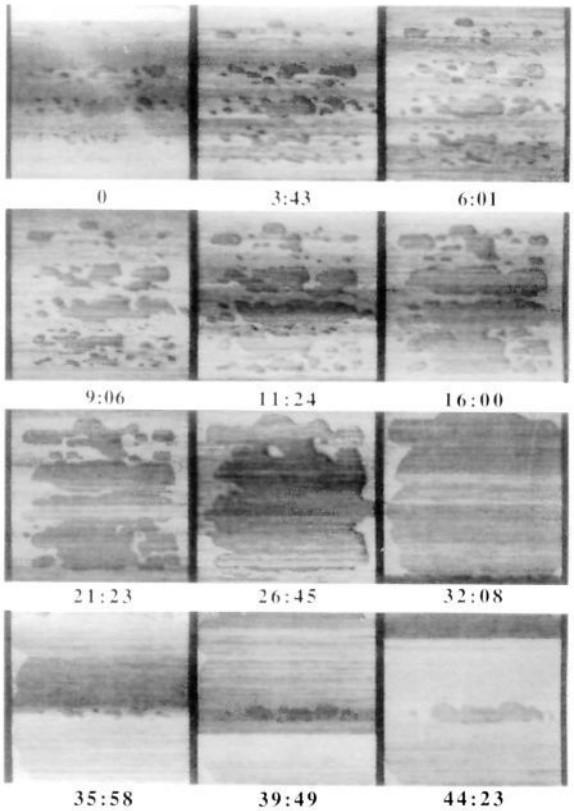

Figure 1. Time evolution of the STM image during the removal of a single molecular layer from the surface of $SnSe_2$ showing the nucleation and growth of holes followed by the nucleation of holes in the next layer. The numbers below the frames show the elapsed time in minutes and seconds with the time of the first frame set arbitrarily to zero. The images are raw data with the STM operating in the constant current mode and the size of the scan is 500 nm. Horizontal banding is due to low-frequency vibrations. The tunneling current was 0.66 nA, and the tunneling bias was 480 mV.

features. Figure 4 shows a 25-nm square 1.2-nm (two *c*-axis units) deep inscribed within a one-layer deep 200-nm square, the smallest feature we have yet produced on $SnSe_2$. These small features grow during imaging making it difficult to determine how small a structure can be made. For example after several scans the feature shown in Figure 4 had grown to beyond 50 nm in diameter.

Substrate Dependence

The etching phenomena is observed on many substrates (metals, semiconductors, and semimetals) with the rates in approximate order InSe > ZrS_2 > $TiSe_2$ > $SnSe_2$ > SnS_2 > $NbSe_2$ > TaS_2 > $MoSe_2$ > WSe_2 > MoS_2, WS_2 > PtS_2 > $ReSe_2$, WTe_2, $MoTe_2$. The latter substrates do not appear to etch at all, and the tungsten and molybdenum selenides and sulfides etch very slowly and only at rather high biases (>1.0 V). We must emphasize the qualitative nature of this etching rate order since the mechanism and controlling processes have not yet been unambiguously identified; crystal perfection is important, and considerable variations in etching rate are observed with different tips. Crystal perfection and purity are probably important factors in controlling the nucleation and growth of holes; however, similar etch rates were observed on the only substrate prepared by both chemical vapor transport and Bridgman growth, $SnSe_2$. The tip composition does not seem to influence the etching since nearly identical results have been observed with either electrochemically etched Pt or W tips or mechanically cut Pt–Ir tips. The bias dependence of the etching rate for $SnSe_2$ was measured by measuring the time from the appearance of hole nucleation to the time of complete removal of a 0.5-μm^2 layer while keeping the tunneling current constant. The data showed no clear trend and was highly scattered with times varying from 5 to 50 min even under identical voltage and

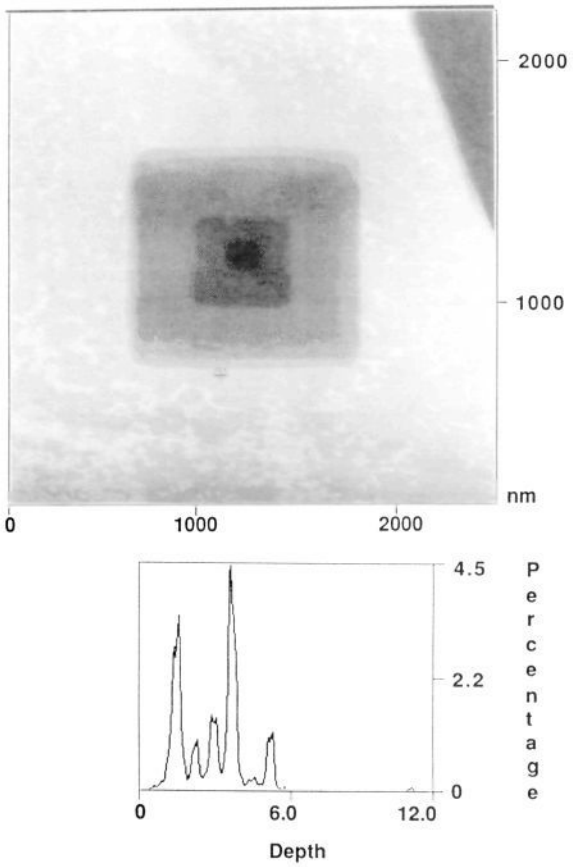

Figure 2. Set of inscribed squares produced by changing the raster size of the STM tip on $SnSe_2$. The larger square is 1 μm on a side and three molecular layers deep, the medium-sized square is 0.5 μm on a side and two molecular layers deep, and the smallest square is 0.2 μm on a side and one layer deep. The lighter spots around the pit are the remnants of a layer removed while imaging the 2400-nm region. The dark area in the upper left is a natural step on the material. The histogram (below) of pixel heights for the central region containing the squares shows peaks for each layer and partial layer which are separated by 0.7 nm, which is within experimental error equal to the *c*-axis dimension of the material (0.614 nm). The tunneling bias and current were the same as those in Figure 1.

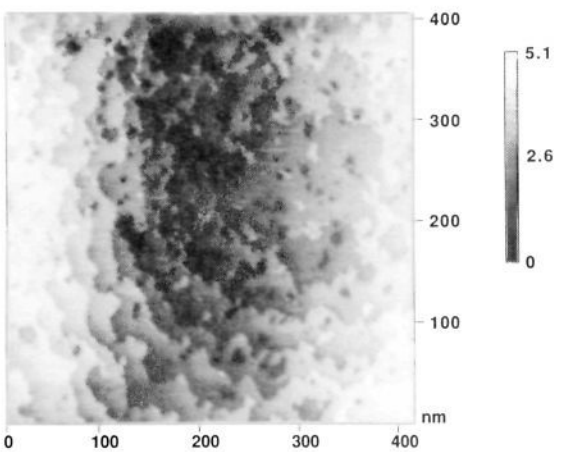

Figure 3. Irregular feature showing many layers produced in $SnSe_2$ by continuous rastering of the tip at a bias of 1420 mV and a current of 0.3 nA over the 400-nm region in an area of the crystal which contained a large number of defects or dopants such that the hole nucleation rate exceeded the hole growth rate. As in Figure 2 the layer height is within experimental error equal to the *c*-axis unit cell of $SnSe_2$.

current conditions. The irreproducibility is perhaps due to the random nature of nucleation events in a given region and/or tip

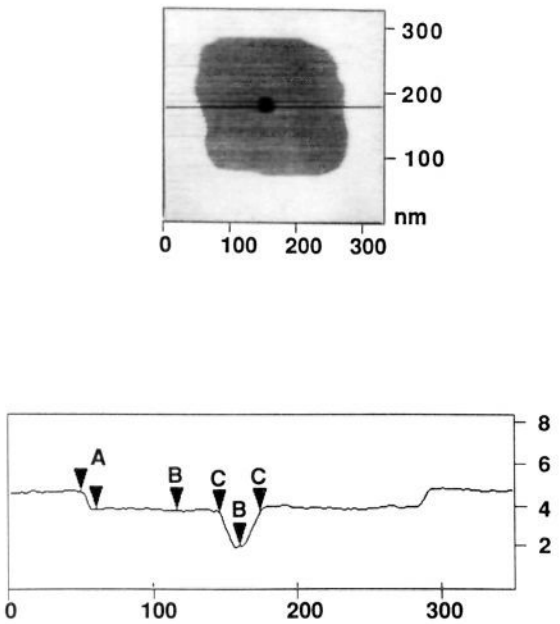

Figure 4. Constant current STM scan of one of the smallest features produced by etching $SnSe_2$. The 25-nm two-layer-deep square in the center was purposely set in the middle of a 200-nm square etched one-layer deep (above). Below is the line scan across the area noted by the line in the STM image above. The vertical distance between the A cursors is 0.75 nm and the B cursors is 1.5 nm. The horizontal distance between the C cursors is 26 nm.

variability, but these experiments did show that the etching process occurs at either negative or positive tip biases. A similar experiment where the bias was held constant and the tunneling current was changed again resulted in highly scattered data.

The etching of $2H_a$-$NbSe_2$ showed a rather surprising nucleation behavior. Figure 5 shows a series of one molecular layer deep triangular etch pits which were observed in the initial stages of etching the surface of $NbSe_2$. The triangular morphology reflects the trigonal prismatic coordination of the metal atom in $NbSe_2$, whereas $SnSe_2$ has metal atoms occupying octahedral sites between the layers. Triangular shapes, and at times shapes suggesting a hexagonal structure, can be observed during the etching of other materials, but they are most distinct in $NbSe_2$ perhaps due to the high quality of these crystals. Characteristically shaped etch pits specific for low index faces of crystals are common when materials are chemically etched; however, such regular structures have not previously been created with the STM.

Possible Etching Mechanisms

We have identified four possible mechanisms for the etching process. The first possibility is that the electric field and/or the current flow between the tip and sample results in the production of reactive species from organic impurities found on surfaces exposed to air or perhaps other reactive species associated with the tip. The radicals thus produced could then diffuse on the surface attacking the most reactive sites (defects for nucleation and exposed edges for hole growth) resulting in volatile products. In the case of $SnSe_2$, alkyltin compounds and H_2Se would be potential products. We tend to disfavor this mechanism because the etching occurs on freshly cleaved surfaces for which we have proven that sticking coefficients for organic impurities are quite low, and no increase in the etching rate with time is observed as would be expected as impurities are accumulated. Etching also occurs in a helium atmosphere. In addition the voltage required for electrochemical generation of reactive radical species would be greater than biases for which etching can still be observed (<100 mV).

The second mechanism for etching is related to the heat or power dissipation in the small region of current flow between tip and sample. One mechanism for deposition of thermal energy into the near surface region of the semiconducting materials would

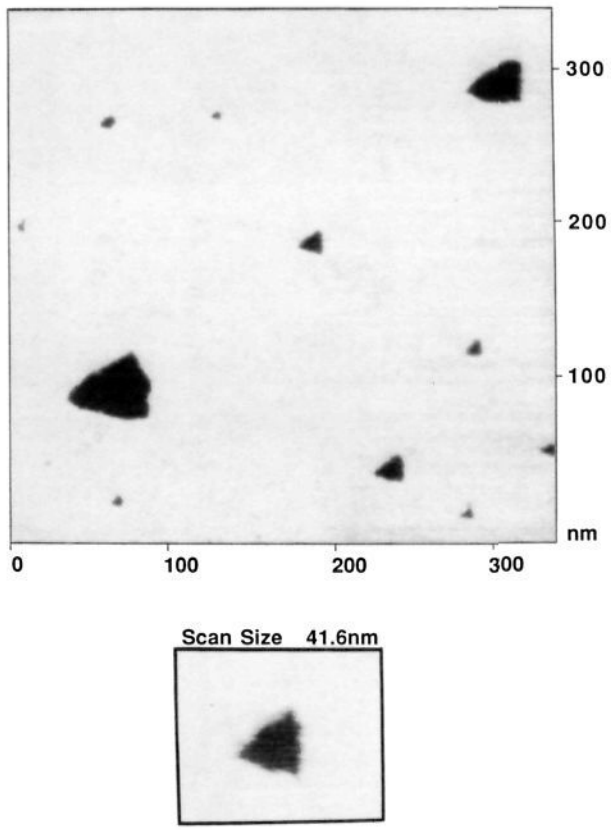

Figure 5. Triangular features appearing during the initial stages of etching the surface of $NbSe_2$. Above is a constant current 350 nm STM scan with the tunneling bias and current of 816 mV and 0.54 nA, respectively. Below is shown a constant current scan of a single triangle (the one near the center of the image above) under the same conditions. A histogram of the pixel heights of the region inside the square shows two peaks separated by 0.7 nm (for the dark and light pixels), which is within experimental error of the single-layer thickness in $NbSe_2$ (0.625 nm).

be from the extremely fast thermalization of electrons injected into the conduction band (or conversely holes in the valence band) well above the band edge. Previous calculations have shown that substantial temperature increases can occur in the STM tip-sample region from electron-hole pair formation in isotropic materials[25] although these calculations were for higher currents and voltages (2.0 V and 10 μA) than those needed to etch our materials. In fact these authors predicted etching may be possible from thermal effects. The dissipation of the excess thermal energy in a two-dimensional material could result in larger surface temperature increases. Phonon coupling in these materials is strongest within the planes resulting in energy primarily remaining near the surface and dissipating at scattering or recombination centers (impurities and defects), perhaps providing enough energy to dissociate the surrounding material into volatile products. A simple calculation shows that the energy throughput during one scan (40 s) of a 0.5-μm square area at 0.5 V and 0.5 nA is 1.5×10^4 times the heat of formation of the top layer of $SnSe_2$. The unknown is what percentage of that energy is actually deposited in the top layer. This electron thermalization hypothesis would predict a voltage threshold for the etching semiconductors as the electron energy goes below the conduction band, such a threshold was not observed for $SnSe_2$. Several metallic compounds (TaS_2 and $NbSe_2$) were also observed to etch where phonon emission from states above the Fermi level would not have a threshold. Thermal mechanisms would predict a linear, square, or fourth power relationship of the etching rate with bias,[25] but due to the large scatter in the data

(25) Flores, F.; Echenique, P. M.; Ritchie, R. H. *Phys. Rev. B* **1986**, *34*, 2899.

no clear dependence on bias or current was observed. In fact etching could still be observed at tunneling currents as low as 0.05 nA and biases as low as 50 mV but at rates less than those at higher values and at the cost of poorer image quality for following the progress of the etching.

A third possible mechanism for the etching process is field-assisted evaporation. This process is well documented in the field ion microscopy literature although some details of the mechanism are still unresolved.[26,27] The process is a result of the polarization of the bonds in a material in the presence of a strong electric field. At very high electric fields atoms can be expelled from the substrate by a mechanism which involves repulsion from its image charge. Although the quantitative aspects of the comparison of field-assisted evaporation from metal tips in UHV and etching of metal chalcogenides by an STM tip in air are a bit tenuous, there are several qualitative aspects which are appealing. The fields in a field ion microscope are generally larger (several V/Å as opposed to the tenths of a V/Å in STM), but residual gases have been observed to assist field evaporation in vacuum systems. The observed field thresholds for evaporation of metals from sharp tips in UHV[26] are in qualitative reverse order to that observed for the STM etching rate of their chalcogenides (W > Re > Pt > Mo > Nb > Zr > Sn > Ti). This order is also roughly the order of the covalency of bonding in the chalcogenides of these metals. Also substantial increases in the nucleation of etch pits and the evaporation rate of an ionic crystal (NaCl) have been observed by application of an electric field of $<3 \times 10^{-5}$ V/Å,[28-30] 10^4 times weaker than the field present between the STM tip and substrate. Field-assisted evaporation would tend to predominant at protrusions and edges where the field is strongest, as is observed, although all the previously discussed mechanisms qualitatively predict this. Evidence for this mechanism comes from the occasional observation, by increasing the scan range, that etching can occur in regions near where the tip is imaging but where there is no tunneling current. When multiple tips are present, one of the tips will dominate the tunneling current, and therefore produce the image; however, a strong electric field can still be present between other microtips and the surface in regions where there is no current flow. The tip-to-tip dependence of the etching rate and the distinctness of the etched features could be explained since the electric field distribution at the tip would be highly affected by the microscopic tip morphology. The observation of etching occurring at both positive and negative biases is difficult to rationalize with this mechanism however.

Abrasion of the substrate via direct tip-sample contact was proposed for the etching observed for $Rb_{0.3}MoO_3$ because in that case etching was only observed at low biases (close tip-sample approach).[16] Several experiments and observations that we have made do not support this mechanism in our case. We have measured the dependence of the tunneling current on tip-sample separation on a $SnSe_2$ sample before commencement of etching, immediately after the nucleation of holes and after removal of several complete layers of $SnSe_2$. Each measurement was the average of 20 tip withdrawal scans and was repeated at several initial currents (0.29, 0.61, and 1.00 nA) and at several biases from 500 to 900 mV. In all cases the current was an exponential function of the tip-sample distance indicating that there is no tip-sample contact. Of course this measurement does not eliminate the possibility of momentary tip-sample contact creating nucleation sites while the tip is rastered. Growth could be accomplished by momentary tip sample contact at the relatively large steps in these materials (5–7 Å) due to the inability of the feedback loop to respond quickly to an abrupt height change. The appearance and growth of the triangular nuclei during etching of $NbSe_2$ (Figure 5) argues against any abrasion mechanism for hole growth since it seems unlikely that such regular features could be continuously carved out or that the surface mobility of $NbSe_2$ units would be sufficiently high to be continually rearranging the surface to form triangular pits. Abrasion would not be expected to show the substrate dependence that we observe where the more covalent materials are less likely to show etching. Also when we purposely or accidentally contact the tip to the surface of the layered materials we always see substantial damage to the surface with very irregular features containing many torn and piled up layers very unlike the purposely etched features.

The actual etching mechanism may be a difficult to unravel combination of any of the four possibilities discussed above; for example, one mechanism may be responsible for nucleation and another for the growth of holes. Mass spectral measurements in UHV may provide additional clues to the mechanism via the ability to measure product ions, neutrals, and any surface contamination. Microanalysis of the tips for product accumulation would be helpful for elucidating the fate of the removed material which does not appear on the substrate near the etched areas; however, both of these techniques may be hindered by the extremely small amounts of material removed from the surface. Atomic force microscopy (AFM) may help elucidate the role of abrasion in etching since the first three mechanisms are not expected to operate in the AFM. Although we have not definitively defined the etching mechanism, we have for the first time been able to view an etching process as it is occurring and have demonstrated the importance of nucleation and growth in the etching process, observations which will have to be accounted for by any proposed mechanism.

Potential Applications and Implications

The etching process immediately suggests several applications. Information storage may be limited by the slow writing rates and inability to find voltage or current values where etching does not occur (the WAM or write always memory!) although atomic force microscopy may provide a nondestructive method for readout. Direct writing of nanoscale electronic components or masks may be possible. The herein described etching process also has implications on the general practice of STM since many substrates and adsorbed species may be difficult to image because of inherently high etching rates. Many 3D materials may also etch under standard tunneling conditions, but it may be difficult to see since their surfaces are usually not as inert or flat as the 2D materials discussed herein. It is our experience that atomic resolution of an easily etched substrate is aided by blunt tips and can be obtained by continual scanning, perhaps until a tip-shaped depression is formed. The bottom of such a depression may be imaged either because a layer has been reached which is deficient in nucleation sites or that the electric field is more uniformly dissipated by a large area of tip-sample close approach when the tip is within the depression.

Experimental Section

The instrument used for all the STM images and the tip-sample separation measurements was the Nanoscope II from Digital Instruments, Santa Barbara, CA. The constant current images were acquired in the 400 × 400 pixel mode with scan rates from 2.5 to 8.7 lines/s. The resulting tip velocities are from 500 to 10000 nm/s. Scanning heads with ranges up to 1 and 7 microns with 150 V applied to the tubular piezoelectric elements were used (Digital Instruments B and D heads, respectively). The integral and proportional gains in the logarithmic feedback mode were from 1 to 3 and 2 to 6, respectively, with a 2D gain of 0.0–0.05. The current and bias values are given in the figure captions of the respective images. Tips were usually platinum and were electrochemically etched in a 5 M KCN, 2 M KOH solution by applying an AC voltage of 0.5–0.6 V with an initial current of 25–45 mA which decays to 0.0 mA when the tip is completed after about 20 min. The tips were then rinsed in water and acetone before use in the STM. Tungsten tips were prepared according to literature procedures[31] and Pt–Ir tips were

(26) Sakurai, T.; Sakai, A.; Pickering, H. W. *Atom-Probe Field Ion Microscopy and Its Applications*; Academic Press, Inc., Harcourt Brace Jovanovich, Publishers: San Diego, CA, 1989; pp 1–48.
(27) Muller, E. W.; Tsong, T. T. *Field Ion Microscopy Principles and Applications*; American Elsevier Publishing Company, Inc.: New York, 1969.
(28) Munir, Z. A.; Nguyen, T. *J. Crystal Growth* **1982**, *57*, 449.
(29) Machida, C. A.; Munir, Z. A. *J. Crystal Growth* **1984**, *68*, 665.
(30) Yacaman, M. J.; Munir, Z. A.; Ocana, T.; Hirth, J. P. *Appl. Phys. Lett.* **1979**, *34*, 727.
(31) Digital Instruments Nanoscope II Instruction Manual; 1990; p 153.

as supplied by the STM supplier. Crystals of $SnSe_2$ and SnS_2 were grown with a Bridgman technique. All the other materials (including some $SnSe_2$) were grown via chemical vapor transport reactions in sealed quartz ampoules with only small variations on published procedures.[32]

(32) Preparation and Crystal Growth of Materials with Layered Structures. In *Physics and Chemistry of Materials with Layered Structures*; Lieth, R. M., Ed.; D. Reidel: Dordrecht, Holland, 1977; Vol. 1.

The crystal samples were mounted to copper disks with Ag epoxy and cleaved via sticky tape before each STM experiment.

Acknowledgment. The experimental assistance of Sue Riggs for STM operation and graphics and R. Scott McLean for assistance in crystal growth is gratefully acknowledged as are many helpful discussions with my colleagues and helpful suggestions of the reviewers.

A Photoelectron–Photoion Coincidence Study of $Fe(CO)_5$

K. Norwood,† A. Ali, G. D. Flesch, and C. Y. Ng*

Contribution from the Ames Laboratory,‡ U.S. Department of Energy, and Department of Chemistry, Iowa State University, Ames, Iowa 50011. *Received March 23, 1990. Revised Manuscript Received June 4, 1990*

Abstract: The photoelectron–photoion coincidence (PEPICO) spectra for $Fe(CO)_n^+$, $n = 0$–5, resulting from the photoionization of $Fe(CO)_5$ have been measured in the wavelength region of 650–1600 Å. The photoionization efficiency and PEPICO measurements provide new values for the ionization energy for $Fe(CO)_5$ and appearance energies for the formation of $Fe(CO)_n^+$, $n = 0$–4. These new values in turn yield values of 17.8 ± 0.9, 25.2 ± 1.1, 25.7 ± 1.4, 41.5 ± 1.6, and 39.3 ± 2.0 kcal/mol for the bond dissociation energies of $CO–Fe(CO)_n^+$, $n = 4$, 3, 2, 1, and 0, respectively. The collision-induced dissociation process, $FeCO^+ + Ar \rightarrow Fe^+ + CO + Ar$, has also been examined as a function of the collision energy and photoionization wavelength used in the preparation of reactant $FeCO^+$. The values for the dissociation energy of $Fe^+–CO$ determined by collision-induced dissociation and by photoionization are in agreement. Similar to the conclusion of the previous PEPICO study of $Cr(CO)_6^+$, the PEPICO data for $Fe(CO)_n^+$, $n = 0$–5, are consistent with a mechanism invoking the sequential fragmentation of CO, except for $Fe(CO)_2^+$, the data of which are in accord with the interpretation that $Fe(CO)_2^+$ may dissociate directly to both $FeCO^+$ and Fe^+.

I. Introduction

Accurate knowledge of the thermochemistry of organometallic compounds is fundamental to the understanding of their bondings and reactivities. The attempt to obtain detailed correlation of thermochemistry and reactivity in simple metal carbonyl ions represents an important goal of modern research in gaseous organometallic ion chemistry.[1,2] Transition-metal carbonyl compounds have been used in many industrial processes such as the vapor deposition of metal films[3] and the catalysis of organic reactions.[4-7] The desire to understand the reaction mechanisms involving intermediate organometallic radicals in these industrial processes has also been the impetus for detailed photochemical studies[8-13] and accurate thermochemical measurements[2,14] of these compounds.

The mass spectrometric technique is a well-established method for measuring the bond dissociation energies of organometallic ions.[15] Many electron impact experiments on $Fe(CO)_5$ have been reported previously.[16-20] These studies provide estimates for the bond dissociation energies of $CO–Fe(CO)_n^+$, $n = 0$–4. The energy resolution used in a photoionization experiment can be significantly superior to that achieved in an electron impact study. A photoionization efficiency study of the processes

$$Fe(CO)_5 + h\nu \rightarrow Fe(CO)_5^+ + e^- \quad (1)$$

$$\rightarrow Fe(CO)_4^+ + CO + e^- \quad (2)$$

$$\rightarrow Fe(CO)_3^+ + 2CO + e^- \quad (3)$$

$$\rightarrow Fe(CO)_2^+ + 3CO + e^- \quad (4)$$

$$\rightarrow FeCO^+ + 4CO + e^- \quad (5)$$

$$\rightarrow Fe^+ + 5CO + e^- \quad (6)$$

has been made.[21] The adiabatic ionization energy (IE) of $Fe(CO)_5$ has also been estimated previously in a photoionization experiment without mass selection.[22] The estimated value for the bond dissociation energy of $Fe^+–CO$ based on the assigned appearance energies (AE) for processes 5 and 6 disagrees with the results of electron impact experiments as well as those of the more recent photodissociation[23] and ligand displacement studies.[24] The photoionization efficiency (PIE) spectra for $Fe(CO)_5^+$ and

† Catron Research Fellow.

‡ Operated for the U.S. Department of Energy by Iowa State University under Contract No. W-7405-Eng-82. This work was supported by the Director for Energy Research, Office of Basic Energy Sciences.

(1) Foster, M. S.; Beauchamp, J. L. *J. Am. Chem. Soc.* **1975**, *97*, 4808.
(2) Connor, J. A. *Curr. Top. Chem.* **1977**, *71*, 71.
(3) Clements, P. J.; Sale, F. R. *Metall. Trans.* **1976**, *7B*, 435.
(4) Bradford, C. W. *Platinum Met. Rev.* **1972**, *16*, 50.
(5) Howe, R. F.; Davidson, D. E.; Whan, D. A. *J. Chem. Soc. Trans. I* **1972**, *68*, 2266.
(6) Howe, R. F. *Inorg. Chem.* **1976**, *15*, 486.
(7) Brenner, A.; Burwell, R. L., Jr. *J. Am. Chem. Soc.* **1975**, *97*, 2565.
(8) Wrighton, M. *Chem. Rev.* **1974**, *74*, 401.
(9) Lewis, K. E.; Golden, D. M.; Smith, G. P. *J. Am. Chem. Soc.* **1984**, *106*, 3905.
(10) Yardley, J. T.; Gitlin, B.; Nathanson, G.; Rosan, A. M. *J. Chem. Phys.* **1981**, *74*, 361, 370.
(11) Ouderkirk, A. J.; Wermer, P.; Schultz, N. L.; Weitz, E. *J. Am. Chem. Soc.* **1983**, *105*, 3354.
(12) Ouderkirk, A. J.; Weitz, E. *J. Chem. Phys.* **1983**, *79*, 1089.
(13) Kotzian, M.; Rosch, N.; Schroder, H.; Zerner, M. C. *J. Am. Chem. Soc.* **1989**, *111*, 7687.
(14) Behrens, R. G. *J. Less-Common Met.* **1977**, *56*, 55.
(15) Litzow, M. R.; Spalding, T. R. *Mass Spectrometry of Inorganic and Organometallic Compounds*; Elsevier: Amsterdam, 1973.
(16) Bidinosti, D. R.; McIntyre, N. S. *Can. J. Chem.* **1967**, *45*, 641.
(17) Foffani, A.; Pignataro, S.; Cantone, B.; Grasso, F. *Z. Physik. Chem.* **1965**, *45*, 79.
(18) Junk, G. A.; Svec, H. J. *Z. Naturforsch.* **1968**, *23B*, 1.
(19) Winters, R. E.; Kiser, R. W. *Inorg. Chem.* **1964**, *3*, 699.
(20) Clements, P. J.; Sale, F. R. *Metall. Trans.* **1976**, *7B*, 171.
(21) Distefano, G. *J. Res. Natl. Bur. Stand.* **1970**, *74A*, 233.
(22) Lloyd, D. R.; Schlag, E. W. *Inorg. Chem.* **1969**, *8*, 2544.
(23) Cassady, C. J.; Freiser, B. S. *J. Am. Chem. Soc.* **1984**, *106*, 6176.
(24) Foster, M. S.; Beauchamp, J. L. *J. Am. Chem. Soc.* **1975**, *97*, 4808.

0002-7863/90/1512-7502$02.50/0